Improved Antenna Efficiency Measurement Uncertainty in a Reverberation Chamber at Millimeter-Wave Frequencies

Damir Senic, Dylan F. Williams, *Fellow, IEEE*, Kate A. Remley, *Fellow, IEEE*, Chih-Ming Wang, Christopher L. Holloway, *Fellow, IEEE*, Zhenchao Yang, *Member, IEEE*, and Karl F. Warnick, *Fellow, IEEE*

***Abstract*— We provide results of antenna radiation and total radiation efficiency at millimeter-wave frequencies gathered with a new open-ended waveguide-plate method that is compared to a well-known two-antenna method. The new method yields improved uncertainty in antenna efficiency measurements. Both methods are based on use of a reverberation chamber. Measurement results are compared to numerical simulations and good agreement (∼3% maximum difference) is achieved. Before performing the efficiency measurements, the chamber configuration was assessed with respect to the Rician K-factor, number of uncorrelated paddle orientations, and coherence bandwidth. We calculated the uncertainty using the NIST microwave uncertainty framework capable of performing parallel sensitivity and Monte Carlo analyses. The framework enables us to capture and propagate the uncertainties in the S-parameter measurements to the final efficiency result. The expanded uncertainty that we achieved for these antenna efficiency measurements is 2.60%.**

***Index Terms*— Antenna radiation efficiency, antenna total radiation efficiency, measurement uncertainty, millimeter wave, open-ended waveguide (OEW), reverberation chamber (RC), wireless systems.**

I. Introduction

IN RECENT years, the massive expansion of wireless technologies has led to high demand for more access to various data content. Consumers expect to have a reliable connection to wireless networks that are capable of transferring large amounts of data. This puts high demands on the wireless telecommunications carriers, in terms of available spectrum and spectral efficacy. The wireless spectrum below 6 GHz is reaching its maximum capacity and, without fundamental changes, likely will not be sufficient to meet future needs. Even with inventive new methods, like multiple-input and multiple-output antenna systems, smaller cells, and complex modulation techniques, the spectrum shortage is evident.

One potential solution to this extreme data growth is broadening the wireless spectrum to higher frequency ranges. The millimeter-wave spectrum is relatively open and this available bandwidth offers opportunities for the development of new wireless technologies.

Frequencies between 10 and 300 GHz are known colloquially as millimeter-wave frequencies [1]. Propagation at these frequencies generally suffers more attenuation due to atmospheric conditions as compared to the UHF spectrum. Therefore, the emphasis on wireless communications in this frequency range will likely be on highly efficient, smart antennas and short-range systems.

Historically, antenna manufacturers have not provided efficiency data. However, numerous wireless tests, especially those involving reverberation chambers (RCs) [2]–[7], require antenna efficiency information, which is then either estimated, or not taken into account. For these reasons, accurate measurements of antenna efficiency are of great interest to the measurement community.

Several techniques have been proposed to measure antenna efficiency in an RC. Most techniques require the use of a reference antenna with a known efficiency (η_{REF}) [8]–[14]. With the reference antenna serving as the transmit antenna, the power at the receive antenna is then measured (P_{REF}). The reference antenna is then replaced by the antenna under test (AUT) and the received power at the same generic receive antenna is measured again (P_{AUT}). The AUT's radiation efficiency is then given by

$$\eta_{\text{AUT}} = \frac{P_{\text{AUT}}}{P_{\text{REF}}}\eta_{\text{REF}}. \tag{1}$$

One main drawback of this method is that it requires knowledge of the reference antenna efficiency.

To avoid the use of a reference antenna with known efficiency, various methods have been proposed [9], [15], [16]. Two identical antennas were used in [9] to calculate the AUT's efficiency. This method was based on determining

Manuscript received November 8, 2016; revised April 5, 2017; accepted May 13, 2017. Date of publication May 25, 2017; date of current version August 2, 2017. This work was supported by U.S. government, not protected by U.S. copyright. *(Corresponding author: Damir Senic.)*

D. Senic is with the Communications Technology Laboratory, National Institute of Standards and Technology, Boulder, CO 80305 USA (e-mail: Damir.Senic@nist.gov).

D. F. Williams, K. A. Remley, and C. L. Holloway are with the Communications Technology Laboratory, National Institute of Standards and Technology, Boulder, CO 80305 USA (e-mail: Dylan.Williams@nist.gov; Kate.Remley@nist.gov; Christopher.Holloway@nist.gov).

C.-M. Wang is with the Statistical Engineering Division, National Institute of Standards and Technology, Boulder, CO 80305 USA (e-mail: chih-ming.wang@nist.gov).

Z. Yang is with the Wireless Technology Development, Starkey Hearing Technologies, Eden Prairie, MN 55344 USA (email: yzcown@gmail.com).

K. F. Warnick is with the Department of Electrical and Computer Engineering, Brigham Young University, Provo, UT 84602 USA (e-mail: warnick@ee.byu.edu).

Color versions of one or more of the figures in this paper are available online at http://ieeexplore.ieee.org.

Digital Object Identifier 10.1109/TAP.2017.2708084

the loss inside the chamber from the chamber's quality (Q) factor. In this paper, the chamber's Q was determined from its decay constant (in the time domain) in which case the antenna efficiency does not have to be considered. The obvious drawback is the requirement for two identical antennas, which can be nontrivial. One-, two-, and three-antenna methods for calculating antenna efficiency based on the chamber decay constant were presented in [16]. Note that previous studies [8]–[15] did not discuss measurement uncertainty.

In this paper, we evaluate the measurement uncertainty for antenna efficiency measurements inside an unloaded RC at millimeter-wave continuous-wave frequencies between 43 and 47 GHz with a novel type of reference antenna. Low uncertainty is especially important in the millimeter-wave frequency range, with the required measurement accuracy increasing linearly with frequency. This is because phase error also increases linearly with frequency.

Only a few studies have been reported on the subject of RC measurements at millimeter-wave frequencies, and none of these dealt with antenna efficiency measurements. Dielectric conductivity and permittivity tests from 30 to 40 GHz were given in [17]. Emission tests of different electrical components from 1 up to 40 GHz have been studied in [18]. In [19], the design and experimental validation of an RC up to 61.5 GHz were presented. Since this frequency range will be used in next-generation high-speed wireless networks [20], RC performance at millimeter-wave frequencies is of great importance.

This paper provides the following original contributions: 1) a new method for measuring waveguide antenna efficiency based on the use of a simple, well-matched, highly efficient reference waveguide antenna that can be easily modeled; 2) a detailed uncertainty analysis made with the NIST microwave uncertainty framework [21]; and 3) antenna efficiency measurements at millimeter-wave frequencies.

This paper is organized as follows: in Section II, the theoretical background for the antenna efficiency measurements is provided. Section III follows with our measurement setup and technique. Section IV verifies the chamber configuration necessary to obtain low uncertainty. Numerical and experimental results are given in Section V. A measurement uncertainty analysis, based on the NIST microwave uncertainty framework, is given in Section VI. Final conclusions are given in Section VII.

II. Antenna Efficiency

Two common metrics that are used to describe antenna efficiency are radiation efficiency (η_{rad}) and realized or total radiation efficiency (η_{tot}) [22]. Throughout the paper, we will use the term total instead of realized radiation efficiency to refer to the latter metric. Antenna radiation efficiency is defined as the ratio of the total power radiated by the antenna to the net power accepted at the input port of the antenna from the connected transmitter. Radiation efficiency includes only the ohmic losses in the antenna [22]. Antenna total efficiency, on the other hand, combines the radiation efficiency of the antenna reduced with its impedance mismatch factor (i.e., by the reflected signal) [22].

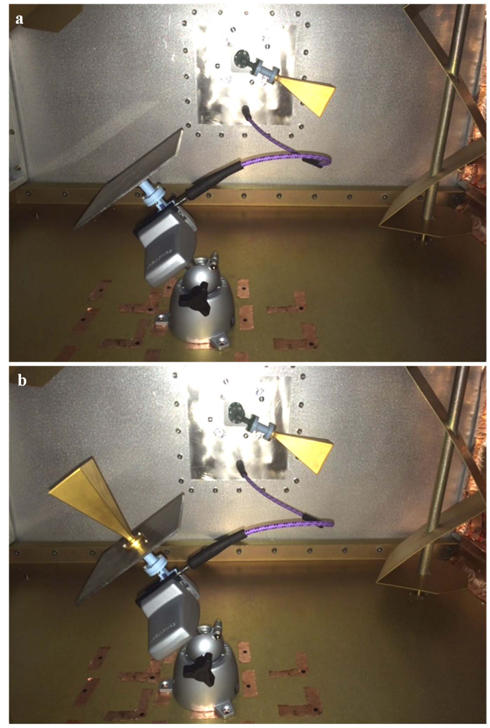

Fig. 1. Measurement setup inside the *RC* for OEW plate method for determining antenna efficiency. (a) OEW plate. (b) Waveguide horn antenna mounted on the OEW plate.

Here, we propose a new type of reference antenna for estimating the efficiency of waveguide-type antennas based on a low-loss metal plate with a waveguide opening machined through it attached to an open-ended waveguide (OEW), [Fig. 1(a)]. We refer to this antenna as the "OEW plate." The plate is made of stainless steel. It includes threaded holes so that a waveguide-type antenna could be connected to the other side [Fig. 1(b)]. The 3.5-mm thick plate utilized in this paper has a WR22 waveguide opening machined through it, and surface dimensions of 140 mm $\times$ 140 mm. This is large enough (21 $\lambda \times 21$ λ at 45 GHz) that the surface currents at the observed frequencies emanating from the waveguide section decay before reaching its edge. Standard OEW test port sections generally have an irregularly shaped, small flange so the coupled surface currents do not decay before reaching the flange edge. The surface currents then wrap around the edge and couple to the back side of the test port flange. Every time currents encounter a discontinuity, energy is radiated. This kind of radiation can cause the existence of undesirable, unstirred energy inside an RC. The plate proposed here reduces these radiation effects.

For a well-stirred RC, the efficiency of an AUT may be found as the relative difference between S-parameters measured for the AUT mounted on the OEW plate (S^{OA}), shown in Fig. 1(b), and the S-parameters measured only for the OEW plate (S^{O}), as shown in Fig. 1(a), as

$$\eta_{\mathrm{tot,\,AUT}} = \frac{\left\langle \left| S_{21}^{\mathrm{OA}} \right|^2 \right\rangle}{\left\langle \left| S_{21}^{O} \right|^2 \right\rangle} \tag{2}$$

$$\eta_{\mathrm{rad,\,AUT}} = \frac{\left\langle \left| S_{21}^{\mathrm{OA}} \right|^2 \right\rangle}{\left\langle \left| S_{21}^{O} \right|^2 \right\rangle \left(1 - \left| \left\langle S_{11}^{\mathrm{OA}} \right\rangle \right|^2\right)} \tag{3}$$

where the brackets denote an ensemble average over paddle orientations. We used the waveguide horn antenna as the AUT.

For validation purposes, we compared our method to a two-antenna method for determining antenna efficiency [16]. The method of [16] does not require a reference antenna and is based on the RC's Q, calculated from the decay constant (τ_{RC}) and angular frequency (ω), $Q = \omega\tau_{RC}$.

Based on the method given in [16], the total radiation efficiency of two antennas placed inside the chamber is given by

$$\eta_{\text{tot, TX}} = \sqrt{\frac{C_{RC}}{\omega\, e_b}\frac{\langle|S_{11,\,s}|^2\rangle}{\tau_{RC}}} \tag{4}$$

$$\eta_{\text{tot, RX}} = \sqrt{\frac{C_{RC}}{\omega\, e_b}\frac{\langle|S_{22,\,s}|^2\rangle}{\tau_{RC}}} \tag{5}$$

where index "s" denotes a stirred component, $C_{RC} = 16\pi^2 V/\lambda^3$ is the chamber constant, and e_b is the enhanced backscatter constant given by [16]

$$e_b = \frac{\sqrt{\langle|S_{11,\,s}|^2\rangle\langle|S_{22,\,s}|^2\rangle}}{\langle|S_{21,\,s}|^2\rangle}. \tag{6}$$

The radiation efficiency of the two antennas in the RC is then given by

$$\eta_{\text{rad,TX}} = \sqrt{\frac{C_{RC}}{\omega\, e_b}\frac{\langle|S_{11,\,s}|^2\rangle_{\text{cor}}}{\tau_{RC}}} \tag{7}$$

$$\eta_{\text{rad, RX}} = \sqrt{\frac{C_{RC}}{\omega\, e_b}\frac{\langle|S_{22,\,s}|^2\rangle_{\text{cor}}}{\tau_{RC}}} \tag{8}$$

where the index designation "cor" refers to the S-parameters corrected for the antenna mismatch, given by

$$\langle|S_{mm,\,s}|^2\rangle_{\text{cor}} = \frac{\langle|S_{mm,\,\text{s}}|^2\rangle}{1 - |\langle S_{mm,\,s}\rangle|^2} \tag{9}$$

and $m = 1$ and 2. After configuring and verifying our RC setup, we compare these methods in Section V.

III. Measurement Setup

We performed all measurements over a frequency range from 43 to 47 GHz using a tabletop-sized RC and a 50-GHz vector network analyzer (VNA). The chamber is equipped with two mechanical stirrers. The larger one rotates about a horizontal (H) axis within a cylindrical volume of 0.6-m height and 0.2-m diameter, while the smaller one rotates about a vertical (V) axis within a cylindrical volume of 0.5-m height and 0.2-m diameter. The RC's inner size is 1 m (l) $\times$ 0.65 m(w) $\times$ 0.55 m(h), which corresponds to an electrical size of approximately 150 $\lambda \times 100\ \lambda \times 80\ \lambda$, at the center frequency of 45 GHz. This is important to emphasize since the high operating frequency results in a large electrical size for the RC, despite its small physical size.

The RC's bulkhead was equipped with two feedthroughs, one in waveguide that was connected to the VNA's port 2 and the other in 2.4 mm coaxial that was connected to the VNA's port 1. Port 2 was terminated with the receive waveguide horn antenna oriented toward the vertical stirrer (see Figs. 1 and 2). We measured the efficiency of two different transmit antennas (AUTs): 1) a waveguide horn antenna shown in [Fig. 2(a)] and 2) a microstrip patch antenna shown in Fig. 2(b). The signal from the 2.4 mm coaxial feedthrough was brought to the AUT via a coaxial cable for the microstrip patch antenna, and via a coaxial cable and coaxial-to-waveguide transition for the waveguide horn antenna. Receive and transmit antennas were oriented away from each other in order to lower the direct signal component between them. The AUTs were oriented toward the horizontal stirrer and positioned at nine different locations within the RC's working volume (see Fig. 3) in order to achieve sufficiently low uncertainty. Key measurement parameters are summarized in Table I.

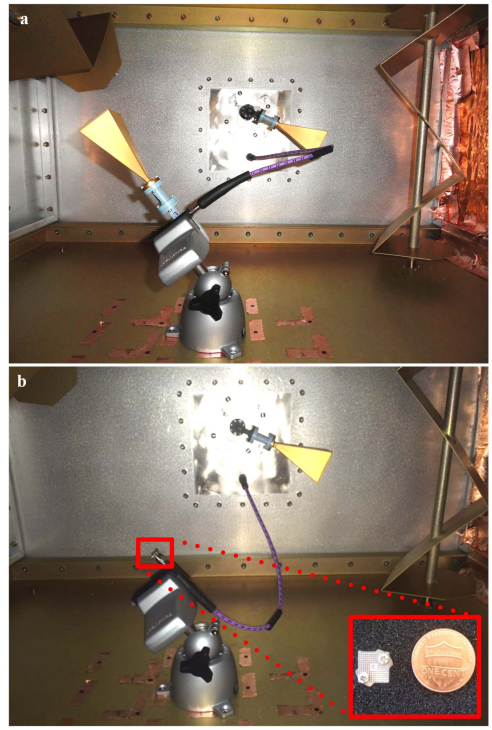

Fig. 2. Measurement setup for the two-antenna method. (a) Waveguide horn antenna; (b) Microstrip patch antenna.

TABLE I
MEASUREMENT PARAMETERS

PARAMETER		VALUE
Frequency range		43 GHz – 47 GHz
VNA IF bandwidth	Calibration	100 Hz
	Measurements	2 kHz
VNA output power level (nominal)		-10 dBm
Paddle step size (V x H)		3.6º x 3.6º
Number of paddle orientations (V X H)		100 x 100

While we used a commercially available WR22 Q-band waveguide horn antenna, the microstrip patch antenna was specifically fabricated in the laboratories of Brigham Young University. The microstrip antenna [23] was designed at 45 GHz based on 0.8128 mm (32 mil) RO4003C substrate and fabricated with standard printed circuit board techniques. The patch size was 1.26 mm $\times$ 1.26 mm, and the ground size was 8 mm $\times$ 8 mm, comparable with the size of a 2.4-mm coaxial connector. The antenna had an omnidirectional

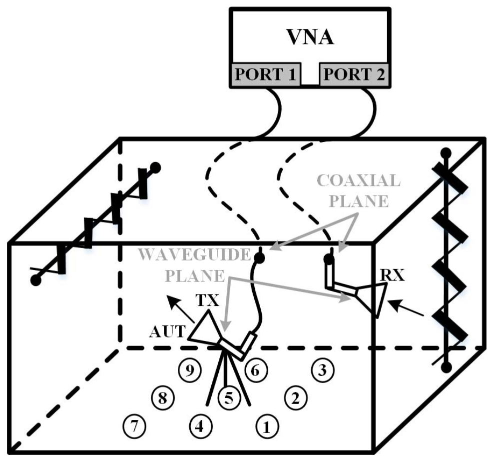

Fig. 3. Diagram of the measurement setup showing the two different calibration planes and the nine AUT locations.

radiation pattern in the patch half-space with maximum gain of 6.8 dB.

S-parameters were measured for 10 000 paddle orientations (100 vertical and 100 horizontal) at each of the nine AUT locations. Since each measurement took approximately 24 h, VNA calibrations were taken at the start and at the end of the 24-h period to verify the calibration stability. We observed the variance of the reflection coefficient (S_{11}) of the "SHORT" standard and the variance of the transmission coefficient (S_{21}) of the "THRU" standard before and after each measurement. The observed calibration deviation in each 24-h period was less than 0.5%.

A diagram of the measurement setup is given in Fig. 3, where we observe two different calibration planes: a waveguide plane at the antenna ports and a coaxial plane at the RC bulkhead ports. Since calibration inside the chamber was physically inconvenient, the calibration plane was transformed from the waveguide reference plane to the coaxial reference plane by embedding the system components through a postprocessor of the NIST microwave uncertainty framework [21].

IV. Configuring the Reverberation Chamber to Achieve Low Measurement Uncertainty

The chamber configuration generally has a significant effect on the measurement uncertainty of the metrics that we are trying to estimate. Parameters that impact overall uncertainty include the type, location, and orientation of the antennas inside the chamber, and the choice of stirring sequence (e.g., mode or paddle and position or antenna stirring). Note that we define "mode-stirring samples" as those arising from stepped-mode operation in this paper.

A. Antenna Placement and Its Impact on the Rician K-Factor

In order to achieve low uncertainty in RC measurements, it is desirable to have a low Rician K-factor associated with the setup. In an RC, the K-factor may be defined as the ratio of unstirred (P_u) to stirred power (P_s). It may be estimated from S-parameters [2] as

$$K = \frac{|\langle S_{21}\rangle|^2}{\langle|S_{21} - \langle S_{21}\rangle^2|\rangle}. \tag{10}$$

TABLE II
K-Factor Measurements at 45 GHz Averaged Over 4-GHz Bandwidth

LOCATION	HORN	PATCH	OEW PLATE
1	-27.29 dB	-23.19 dB	-23.32 dB
2	-27.26 dB	-22.30 dB	-22.45 dB
3	-27.85 dB	-22.18 dB	-23.03 dB
4	-29.40 dB	-22.86 dB	-22.98 dB
5	-29.81 dB	-23.33 dB	-23.99 dB
6	-28.90 dB	-20.83 dB	-22.64 dB
7	-27.21 dB	-22.67 dB	-23.04 dB
8	-28.89 dB	-22.38 dB	-22.85 dB
9	-28.54 dB	-21.97 dB	-23.12 dB
Average	-28.25 dB	-22.29 dB	-23.03 dB

To achieve the lowest uncertainty without position stirring, the K-factor should be as low as possible. High K-factors are directly related to the lack of spatial uniformity of the average fields within the chamber. Prior work on the K-factor in RC measurements can be found in [2]–[7].

The K-factor depends on several different factors including antenna type, location and orientation, and the chamber's loading. In this paper, we considered only an unloaded chamber with fixed optimum antenna orientations (i.e., aimed away from each other) that would yield the lowest K-factor.

K-factor results measured for the three different transmit antenna types at the nine different antenna locations averaged over a 4-GHz frequency band are given in Table II. K-factor uncertainties can be found in [6]. The receive antenna was a waveguide horn in all three cases. Since our OEW plate and the patch antenna have wider main radiation lobes than the more directional horn antenna, they cause more energy to couple to the receive antenna before interacting with paddles. Therefore, we expect that they have larger K-factor values than the waveguide horn antenna. However, all three antennas produced sufficiently low K-factor values to ensure that the stirred energy component dominates throughout our working volume.

B. Number of Uncorrelated Mode-Stirring Samples and Coherence Bandwidth

Uncorrelated mode-stirring samples in a mode-stirring sequence and uncorrelated frequency samples may be used to readily obtain the uncertainty in an estimate of a measured quantity. Methods for determining the effective number of uncorrelated paddle orientations can be found in [24]–[29].

To calculate the number of uncorrelated paddle orientations, we performed measurements at 900 vertical stirrer orientations (0.4° paddle step). The vertical and horizontal stirrers' autocorrelation (r) was computed for the OEW plate, the waveguide horn, and the microstrip patch antennas as

$$r(\Delta n) = \frac{\left\langle S_{21n}(f_m) S^*_{21n+\Delta n}(f_m)\right\rangle_n - |\langle S_{21n}(f_m)\rangle_n|^2}{\langle|S_{21n}(f_m)|^2\rangle_n - |\langle S_{21n}(f_m)\rangle_n|^2} \tag{11}$$

where we used the complex S_{21} parameter at the mth frequency point f_m, nth stirrer orientation, and Δn stirrer step. The coherence angle (ϕ) [26], [30], [31] for a $1/e$ threshold [13] was $\sim$1.4° (257 uncorrelated orientations) for the

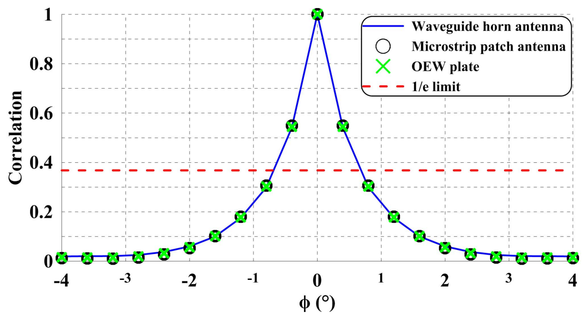

Fig. 4. Correlation between different paddle orientations for the vertical stirrer calculated for the three different transmit antennas, and compared to the $1/e$ limit.

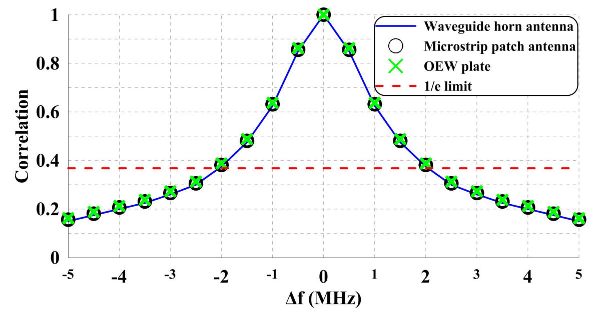

Fig. 5. Coherence bandwidth calculated for the three different transmit antennas, averaged over 10 000 paddle orientations, and compared to the $1/e$ limit.

vertical stirrer shown in Fig. 4 and 1.5° (240 uncorrelated orientations) for the horizontal stirrer. We compared this to the method of [29], in which the optimal threshold for the autocorrelation function depends on the number of measurement samples. Following approach given in [29], we determined the threshold to be 0.4 for 900 stirrer orientations, which resulted in a coherence angle of ~1.3° and 276 uncorrelated orientations for the vertical stirrer and 1.4° and 257 uncorrelated orientations for the horizontal stirrer. The reason horizontal stirrer produced smaller number of uncorrelated measurements than vertical is due to its smaller size. The coherence angle and number of uncorrelated measurements are similar using both methods.

The coherence bandwidth (CBW) represents the average bandwidth over which frequencies have correlation above a specified threshold. The CBW can be determined from the autocorrelation function (R) of the frequency-domain transfer function S_{21} [13], [32], [33] as

$$R(\Delta f_i, n_i) = \sum_{j=1}^{m} S_{21}(f_j, n_i) S_{21}^{*}(f_j + \Delta f_i, n_i) \tag{12}$$

where $S_{21}(f, n)$ corresponds to the measured complex S_{21} at frequency step f_j with m frequency points measured within the bandwidth of interest, Δf corresponds to one of several frequency offsets over the bandwidth of interest, the index n_i is the mode-stirring sample (out of N), and the asterisk denotes complex conjugation.

The autocorrelation function was calculated in the frequency range 43–47 GHz with 32 001 frequency points for the OEW plate, waveguide horn, and microstrip patch antennas. The results show a CBW of approximately 4 MHz for a $1/e$ threshold [13] for all antenna types (see Fig. 5). This CBW resulted in 1000 uncorrelated frequency samples within the observed frequency range.

Based on the coherence angle and CBW obtained, we set the number of paddle orientations and number of frequency points in the observed frequency range.

V. Antenna Efficiency Results

As described in Section II, our method for determining antenna efficiency is based on the reference antenna described above, consisting of a low-loss plate attached to the OEW flange, with a calculable, high efficiency. In this section, we determine the OEW plate efficiency based on analytical and numerical calculations. Numerical results were obtained with full-wave, finite-element method (FEM)-based software capable of performing high-frequency electromagnetic field simulations.

A. OEW Plate Efficiency

To determine the efficiency of the OEW plate introduced in Section II, we need to calculate the ohmic losses in the WR22 waveguide section and plate.

For the numerical simulations, the ohmic losses were calculated from the real part of the Poynting vector. For a 1-W input power, the numerical software calculated the waveguide wall loss value due to the dominant mode as 3.29 mW and total loss value as 3.74 mW.

We next consider an analytic solution for the ohmic loss in the OEW plate. If the magnetic field is known on both the waveguide walls and the plate, the reference antenna ohmic losses can be approximated by [34]

$$P_L = \frac{R_S}{2} \int |H|^2 dS \tag{13}$$

where dS is the surface area of the waveguide walls and plate, H is the magnetic field on the surfaces, and R_S is the real part of the surface impedance given by [34]

$$R_S = \sqrt{\frac{\omega\mu}{2\sigma}} \tag{14}$$

where μ is the material permeability and σ is the material conductivity. The approximation in (13) neglects the edge effects, causing the estimate of the surface impedance (14) to be invalid near the sharp corners; i.e., near the plate's edge [35]. Surfaces were considered as ideal without any roughness.

Motivated by the discussion given above, we consider the waveguide wall and the plate separately. In general, the magnetic field on the plate is not easily obtained and we will neglect it here. The magnetic field on the waveguide wall has contributions from both the fundamental TE_{10} mode and from higher-order modes due to the discontinuity at the waveguide-plate edge. In this analysis, we will neglect the higher-order mode contributions to the losses and calculate only the losses due to the forward and backward propagating TE_{10} mode in the waveguide.

By evaluating (13) for the TE_{10} mode, the power loss per unit length may be given by [34]

$$P_L = P_{\text{in}} \frac{1}{ab} \frac{2Z_{\text{TE}}}{\omega^2 \mu^2} \sqrt{\frac{\omega\mu}{2\sigma}} \left(\frac{2\pi^2 b}{a^2} + a\omega^2 \mu\varepsilon \right) L \tag{15}$$

where P_{in} is the input power, a and b are the waveguide dimensions, Z_{TE} is the impedance of the TE_{10} mode, ε is the permittivity, and L is the waveguide length.

Power launched at the antenna port propagates toward the plate. A portion of the energy is radiated and a portion is reflected back to the waveguide. Therefore, the total loss (P_T) for both the forward and backward propagating TE_{10} mode in the waveguide wall is given by [34]

$$P_{\text{T}} = P_{\text{L}}(1 + |\Gamma|^2) \tag{16}$$

where Γ is the reflection coefficient for the TE_{10} mode at the plate. This can be approximated by [36], [37]

$$\Gamma = \frac{1 - Y}{1 + Y} \tag{17}$$

where

$$\begin{aligned} Y = &\frac{2j}{\pi ab\sqrt{k_0^2 - \left(\frac{\pi}{a}\right)^2}} \\ &\cdot \int_0^a \int_0^b (b - x) \left[A(a - y) \cos\frac{\pi y}{a} + \frac{a}{\pi} B \sin\frac{\pi y}{a} \right] \\ &\times \frac{e^{-jk_0 r}}{r} dx dy \end{aligned} \tag{18}$$

and

$$A = k_0^2 + \left(\frac{\pi}{a}\right)^2, \quad B = k_0^2 - \left(\frac{\pi}{a}\right)^2, \quad r = \sqrt{x^2 + y^2} \tag{19}$$

where j is the imaginary operator and k_0 is the wavenumber.

From (16), we calculated the total loss for the forward and backward waves in the WR22 waveguide to be 3.29 mW for 1-W input power. Note the good agreement with FEM simulation results (also 3.29 mW), given above. This analytical calculation neglects the loss due to the higher-order modes and loss in the plate.

The calibration for the OEW plate was performed by placing calibration standards on the side of the OEW plate away from the waveguide flange. As a result, the dominant-mode loss was calibrated out from the total loss. Thus, only losses originating from higher-order modes and from the plate were present. By subtracting the numerically or analytically obtained waveguide dominant-mode loss (3.29 mW) and not subtracting the plate and higher-order mode from the total loss obtained by the numerical simulations (3.74 mW), we calculated $P_L = 0.45$ mW.

From this loss calculation, we can estimate the reference antenna (OEW plate) radiation efficiency as

$$\eta_{\text{rad,REF}} = \frac{P_{\text{ac}} - P_L}{P_{\text{ac}}} \tag{20}$$

where P_{ac} is the power accepted by the OEW plate, $P_{\text{ac}} = P_{\text{in}}(1 - |\Gamma|^2)$. The P_{ac} obtained by numerical simulations was 958.97 mW and the one from the analytical approach was 940 mW. By substitution of the above given values for P_L and P_{ac} into (20), we calculated the numerically obtained radiation efficiency as 99.96%, while the analytically obtained efficiency was 99.95%.

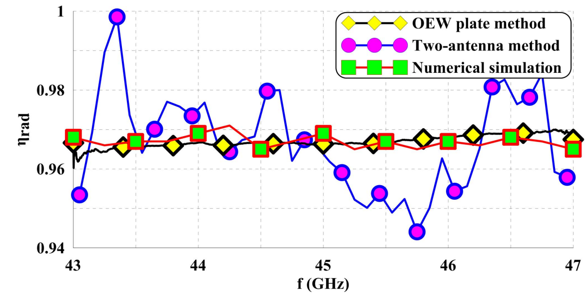

Fig. 6. Waveguide horn antenna radiation efficiency results averaged over the nine antenna locations showing good agreement (~3% maximum difference) between the two measurement methods and simulations.

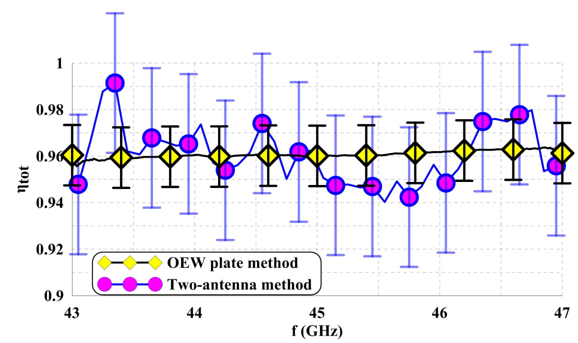

Fig. 7. Waveguide horn antenna total radiation efficiency results averaged over the nine antenna locations showing good agreement (~3% maximum difference) between the two measurement methods. Error bars give the expanded ($k = 2$) measurement uncertainty values for the two different measurement methods.

B. Waveguide Horn Antenna Efficiency

We compare different methods (two measurements and one simulation) to obtain the efficiencies of the waveguide horn antenna. The first measurement method is based on the highly efficient (99.95%) OEW plate given in Sections II and V-A. The second, two-antenna method, also described in Section II, was used for the purpose of comparison. The two-antenna method requires knowledge of the chamber's decay constant, which can be calculated from S_{11} [33]. Finally, we performed numerical simulations based on the FEM to compute the radiation efficiency of the waveguide horn antenna.

The measurement-based radiation efficiency was calculated from (3) and (7) after correcting for the antenna mismatch. By not correcting for the antenna mismatch, the total radiation efficiency can be calculated from (2) and (4). The results for the radiation efficiency of the waveguide horn antenna are given in Fig. 6. FEM-based numerical results show excellent agreement (~0.5% maximum difference) with the OEW-plate-based measurement results, while good agreement (~3% maximum difference) can be observed for the two-antenna method.

Total radiation efficiency results for the waveguide horn antenna obtained from the OEW plate and two-antenna

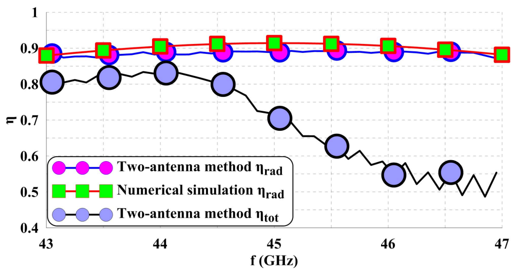

Fig. 8. Microstrip patch antenna radiation and total radiation efficiency results averaged over nine antenna locations.

TABLE III

RADIATION EFFICIENCY AND TOTAL RADIATION EFFICIENCY RESULTS AVERAGED OVER NINE ANTENNA LOCATIONS AND 4-GHz BANDWIDTH

EFFICIENCY	METHOD	HORN η (%)	PATCH η (%)
Radiation	Two-antenna	96.68	88.62
	OEW plate	96.70	/
	Simulations	96.70	90.14
Total radiation	Two-antenna	96.08	81.81*
	OEW plate	96.07	/
	Simulations	/	/

*Data refer to patch antenna total radiation efficiency averaged over a 43 GHz – 44.5 GHz subband, computed before antenna impedance mismatch lowers the antenna efficiency.

methods are given in Fig. 7. Good agreement (~3% maximum difference) is noted when comparing these two different methods. Note that numerical simulations provide us only radiation efficiency, and, hence, cannot be included in Fig. 7.

The average (over paddle orientations, nine locations within the RC, 4-GHz frequency band, and different methods) radiation efficiency of the waveguide horn antenna was ~96.69%, while the average total radiation efficiency was ~96.08%.

C. Microstrip Patch Antenna Efficiency

In the previous section, we showed good agreement between the OEW plate and two-antenna measurement methods. Since the OEW plate method for determining antenna efficiency only applies to waveguide-type antennas, in this section we will show the efficiency results for a microstrip patch antenna obtained from the two-antenna method and compared to numerical simulations.

The radiation efficiency and the total radiation efficiency for the microstrip patch antenna are shown in Fig. 8 as a function of frequency. We observe good agreement (~3% maximum difference) between radiation efficiency results obtained from the two-antenna method and the numerical simulations. The average (over paddle orientations, nine locations, 4-GHz frequency band, and two different methods) radiation efficiency of the microstrip patch antenna is ~89.38%. Fig. 8 shows that the patch antenna has a much lower total radiation efficiency above 44.5 GHz. The reason for this is poor impedance matching above 44.5 GHz and high substrate losses. Due to that reason, we report here the patch antenna's total radiation efficiency in a subband from 43 to 44.5 GHz as 81.81%. The antenna would likely be used in a subband such as this. Efficiency results for the waveguide horn and microstrip patch antennas, averaged over 4-GHz bandwidth and over nine antenna locations, are summarized in Table III.

The maximum difference in averaged efficiency results among the different methods was 1.5%. In the next section, we present the measurement uncertainty budget and determine the significance of this difference.

VI. MEASUREMENT UNCERTAINTY

In [6] we provided an uncertainty budget based on the same low Rician K-factor setup. In that work, we performed a significance test which determined that the uncertainty due to the finite number of mode-stirring measurement samples had the most significant impact on the overall uncertainty, as compared to the uncertainty due to the lack of spatial uniformity [38], [39]. In that work, the uncertainty due to the finite number of mode-stirring measurement samples in [6] for the same setup used here was calculated with an analytic formulation. Here, we provide the uncertainty results from the NIST Microwave Uncertainty Framework [21], [40], calculated using a Monte Carlo approach, and compare them to the analytic result from (21).

Assuming that the spatial uniformity is good and the same number of uncorrelated stirrer orientations N are used for both the reference and AUT measurements, the uncertainty due to the finite number of mode-stirring samples for a perfectly efficient reference antenna would combine in a root-sum-of-squares fashion yielding [41]

$$u = \sqrt{\frac{2}{N}}. \tag{21}$$

Thus, the uncertainty of traditional efficiency measurements (1) based on 10 000 paddle orientations calculated from (21) would be 1.41%.

The NIST Microwave Uncertainty Framework [21] was used to calibrate the measurements and to calculate uncertainties in the corrected result. The Framework assigns the uncertainties and probability distributions to error mechanisms in the calibration, and propagates the associated uncertainties to the end result. It represents the resulting errors as perturbed measurement vectors that are propagated from one calculation step to the next. This enables uncertainties to be correctly correlated throughout the calculations even when the same uncertainty mechanism is present at different steps of the calculation.

The approach is based on parallel sensitivity and Monte Carlo analyses that enable us to capture and propagate the uncertainties of S-parameter measurements and find the correlation between them. By identifying the error mechanisms in the calibration standards, we can determine the correlations between the S-parameters across frequencies, which can then be propagated into the measurement uncertainties.

The uncertainty due to the finite number of mode-stirring measurement samples over the observed frequency range for the antenna total radiation efficiency measurements based on the OEW plate method at the nine different antenna

TABLE IV

UNCERTAINTY DUE TO FINITE NUMBER OF MODE-STIRRING SAMPLES ESTIMATED BY THE NIST MICROWAVE UNCERTAINTY FRAMEWORK FOR TOTAL RADIATION EFFICIENCY

ANTENNA LOCATION	UNCERTAINTY (%)		
	MINIMUM	MEDIAN	MAXIMUM
1	0.92	1.17	1.57
2	0.94	1.17	1.48
3	0.97	1.17	1.55
4	0.95	1.16	1.54
5	0.92	1.14	1.41
6	0.96	1.20	1.52
7	0.96	1.20	1.52
8	0.94	1.18	1.51
9	0.97	1.20	1.55

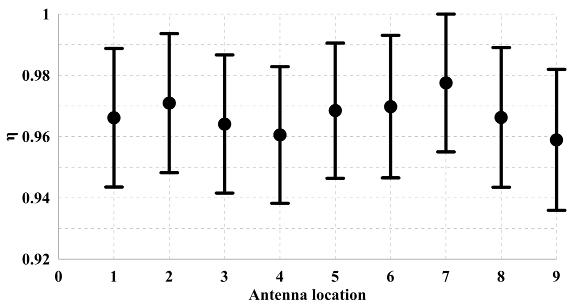

Fig. 9. Horn antenna total radiation efficiency results based on OEW plate method at the nine different antenna locations with the expanded uncertainty error bars.

locations is given in Table IV. The median uncertainty value varied between 1.14% and 1.20% with respect to the antenna location, which is in good agreement with the uncertainty due to the finite number of mode-stirring samples of 1.12% obtained in [6] and based on the same low K-factor setup. The maximum uncertainty value varied between 1.41% and 1.57% with respect to the antenna location.

The antenna total radiation efficiency results obtained from the OEW plate method at the nine different antenna locations, along with the expanded uncertainty ($\pm 2 \times u_{\text{median}}$) from Table IV, are given in Fig. 9. Since the expanded uncertainty error bars overlap for different antenna locations, we may conclude that the component of the uncertainty due to lack of spatial uniformity is not significant. Therefore, as in [6], we can choose any antenna location as representative.

In addition to the uncertainty due to the finite number of mode-stirred measurement samples, we also calculated the uncertainty due to the cable movement. Because the transmit antenna was positioned at nine different locations inside the chamber after the calibration was performed, cable movement represents a potential source of uncertainty. To estimate this component of uncertainty, we measured the "THRU" standard nine times, each time moving the cable to different positions, as shown in Fig. 3, and calculated the median of this uncertainty to be 0.03%. The reason for such low uncertainty due to cable movement was in the fact that efficiency is a power-related measurement and, thus, the phase change that arises from cable movement does not significantly impact the result.

For the efficiency measurements based on the OEW plate, another component of uncertainty is related to the loss in

TABLE V

OEW PLATE MEASUREMENTS UNCERTAINTY BUDGET FOR TOTAL RADIATION EFFICIENCY

Uncertainty source	Value (%)	Combined (%)	Expanded (k=2) (%)
Finite number of mode-stirring samples	1.20	1.30	2.60
Calibration stability	0.5		
Cable movement	0.03		
Plate loss	0.05		

the plate. For the case when there is no AUT connected to the OEW plate, the currents emanate from the waveguide section and are coupled to the plate. On the other hand, when there is an AUT attached to the reference antenna, there is no current directly induced on the plate. In Section V-A. we estimated that this effect causes only 0.05% uncertainty in estimating the AUT's radiation efficiency. The uncertainty budget for total radiation efficiency is given in Table V. The expanded ($k = 2$) uncertainty for the OEW plate method was 2.6%, whereas we calculated 6% for the two-antenna method [16]. The expanded uncertainty results are given as the error bars in Fig. 7 for both methods. An obvious advantage of the OEW plate method is the lower measurement uncertainty. The efficiency results obtained from both methods agree within their estimated uncertainty.

VII. CONCLUSION

In this paper, we presented measurement and simulation results for antenna radiation efficiency and total radiation efficiency at millimeter-wave frequencies. Prior to the efficiency measurements, we evaluated our unloaded reverberation-chamber setup with respect to the K-factor, number of uncorrelated mode-stirring samples, and CBW. Two different antenna types were evaluated, a 22-dB waveguide horn and a 6.8-dB microstrip patch antenna.

To determine the efficiency of the waveguide horn antenna, we introduced a reference antenna based on a low-loss metallic plate with a machined waveguide opening attached to the flange of an OEW. The plate was fabricated in such a way that a waveguide horn antenna could be connected to it. The efficiency of the horn antenna was then calculated as the relative difference in S-parameters measured for the antenna mounted on the OEW plate and the S-parameters measured only for the OEW plate. We verified the method by comparing it to the two-antenna method. The measurement results were then compared to numerical simulations. Good agreement between these three different methods was achieved.

We computed the measurement uncertainty using the NIST microwave uncertainty framework. This software package is capable of assigning uncertainties and probability distributions to error mechanisms in the calibration and propagating the associated uncertainties to the end result. The expanded uncertainty (2.6%) achieved was in excellent agreement with the uncertainty estimated in our prior work [6] based on empirical methods [38], [40], and was lower that the expanded uncertainties for the two-antenna method (6%) given in [16]. Note that the efficiency results obtained for all methods were within estimated measurement uncertainty. These results are very important for future technologies that rely on high measurement accuracy.

The use of RCs as test environments at millimeter-wave frequencies is advantageous as compared to anechoic chambers. Tests at millimeter-wave frequencies performed in anechoic chambers can be rather challenging due to need for subwavelength sampling. This can be especially cumbersome for highly directional antennas such as waveguide horns. On the other hand, the large electrical size of the RC actually helps to create a well-stirred environment due to the many modes that exist inside the chamber. Future work will assess whether chamber loading, required for tests involving demodulation of communication signals, may present a challenge. Obtaining spatial uniformity of the averaged fields in the loaded chamber to achieve low uncertainty could be an issue due to locally high peaks and nulls.

Regardless, the proposed OEW plate method for determining antenna efficiency based on a low loss, calculable reference antenna does have very low uncertainty. Thus, it may be appropriate for use as a standard measurement method for waveguide-type antennas in electromagnetic compatibility and wireless applications.

REFERENCES

[1] T. S. Rappaport, R. W. Heath, Jr., R. C. Daniels, and J. N. Murdock, *Millimeter Wave Wireless Communications*. Englewood Cliffs, NJ, USA: Prentice Hall, 2015.

[2] C. L. Holloway, D. A. Hill, J. M. Ladbury, P. F. Wilson, G. Koepke, and J. Coder, "On the use of reverberation chambers to simulate a Rician radio environment for the testing of wireless devices," *IEEE Trans. Antennas Propag.*, vol. 54, no. 11, pp. 3167–3177, Nov. 2006.

[3] C. Lemoine, E. Amador, and P. Besnier, "On the K-factor estimation for Rician channel simulated in reverberation chamber," *IEEE Trans. Antennas Propag.*, vol. 59, no. 3, pp. 1003–1012, Mar. 2011.

[4] P. S. Kildal, X. Chen, C. Orlenius, M. Franzen, and C. S. L. Patane, "Characterization of reverberation chambers for OTA measurements of wireless devices: Physical formulations of channel matrix and new uncertainty formula," *IEEE Trans. Antennas Propag.*, vol. 60, no. 8, pp. 3875–3891, Aug. 2012.

[5] C. M. J. Wang *et al.*, "Parameter estimation and uncertainty evaluation in a low Rician K-factor reverberation-chamber environment," *IEEE Trans. Electromagn. Compat.*, vol. 56, no. 5, pp. 1002–1012, Oct. 2014.

[6] D. Senic *et al.*, "Estimating and reducing uncertainty in reverberation-chamber characterization at millimeter-wave frequencies," *IEEE Trans. Antennas Propag.*, vol. 64, no. 7, pp. 3130–3140, Jul. 2016.

[7] K. A. Remley *et al.*, "Configuring and verifying reverberation chambers for testing cellular wireless devices," *IEEE Trans. Electromagn. Compat.*, vol. 58, no. 3, pp. 661–672, Jun. 2016.

[8] D. A. Hill, *Electromagnetic Fields in Cavities*. Piscataway, NJ, USA: Wiley, 2009.

[9] H. G. Krauthäuser and M. Herbrig, "Yet another antenna efficiency measurement method in reverberation chambers," in *Proc. IEEE Int. Symp. Electromagn. Compat.*, Jul. 2010, pp. 536–540.

[10] M. Piette, "Antenna radiation efficiency measurements in a reverberation chamber," in *Proc. Asia–Pacific Radio Sci. Conf.*, Aug. 2004, pp. 19–22.

[11] P.-S. Kildal and K. Rosengren, "Correlation and capacity of MIMO systems and mutual coupling, radiation efficiency, and diversity gain of their antennas: Simulations and measurements in a reverberation chamber," *IEEE Commun. Mag.*, vol. 42, no. 12, pp. 104–112, Dec. 2004.

[12] A. Khaleghi, "Time-domain measurement of antenna efficiency in reverberation chamber," *IEEE Trans. Antennas Propag.*, vol. 57, no. 3, pp. 817–821, Mar. 2009.

[13] *EMC, Part 4: Testing and Measurement Techniques; Section 21: Reverberation Chamber Test Methods*, document IEC 61000-4-21, Int. Electrotech. Commun., Geneva, Switzerland, 2011.

[14] A. A. H. Azremi, H. G. Shiraz, and P. S. Hall, "Reverberation chamber for efficiency measurement of small antennas," in *Proc. Int. Conf. Comput., Commun., Signal Process. Special Track Biomed. Eng.*, Nov. 2005, pp. 25–29.

[15] P. Hallbjörner, "Reflective antenna efficiency measurements in reverberation chambers," *Microw. Opt. Technol. Lett.*, vol. 30, no. 5, pp. 332–335, Sep. 2001.

[16] C. L. Holloway, H. A. Shah, R. J. Pirkl, W. F. Young, D. A. Hill, and J. Ladbury, "Reverberation chamber techniques for determining the radiation and total efficiency of antennas," *IEEE Trans. Antennas Propag.*, vol. 60, no. 4, pp. 1758–1770, Apr. 2012.

[17] P. Hallbjorner, U. Carlberg, K. Madsen, and J. Andersson, "Extracting electrical material parameters of electrically large dielectric objects from reverberation chamber measurements of absorption cross section," *IEEE Trans. Electromagn. Compat.*, vol. 47, no. 2, pp. 291–303, May 2005.

[18] X. Zhou, J. Li, H. Fan, A. Bhobe, P. Sochoux, and J. Yu, "High-frequency EMC design verification through full-wave simulations and measurements in reverberation chamber," in *Proc. IEEE Int. Symp. Electromagn. Compat.*, Denver, CO, USA, Aug. 2013, pp. 299–305.

[19] A. K. Fall, P. Besnier, C. Lemoine, M. Zhadobov, and R. Sauleau, "Design and experimental validation of a mode-stirred reverberation chamber at millimeter waves," *IEEE Trans. Electromagn. Compat.*, vol. 57, no. 1, pp. 12–21, Feb. 2015.

[20] C. Park and T. S. Rappaport, "Short-range wireless communications for next-generation networks: UWB, 60 GHz millimeter-wave WPAN, and ZigBee," *IEEE Trans. Wireless Commun.*, vol. 14, no. 4, pp. 70–78, Aug. 2007.

[21] D. F. Williams, *NIST Microwave Uncertainty Framework (Beta Version)*. Boulder, CO, USA: NIST, Jun. 2014. [Online]. Available: http://www.nist.gov/ctl/rf-technology/related-software.cfm

[22] *IEEE Standard for Definitions of Terms for Antennas*, IEEE Standard 145-2013, Dec. 2013.

[23] Z. Yang and K. F. Warnick, "Multiband dual-polarization high-efficiency array feed for Ku/reverse-band satellite communications," *IEEE Antennas Wireless Propag. Lett.*, vol. 13, pp. 1325–1328, 2014.

[24] J. G. Kostas and B. Boverie, "Statistical model for a mode-stirred chamber," *IEEE Trans. Electromagn. Compat.*, vol. 33, no. 4, pp. 366–370, Nov. 1991.

[25] C. Lemoine, P. Besnier, and M. Drissi, "Estimating the effective sample size to select independent measurements in a reverberation chamber," *IEEE Trans. Electromagn. Compat.*, vol. 50, no. 2, pp. 227–236, May 2008.

[26] K. Madsen, P. Hallbjörner, and C. Orlenius, "Models for the number of independent samples in reverberation chamber measurements with mechanical, frequency, and combined stirring," *IEEE Antennas Wireless Propag. Lett.*, vol. 3, no. 1, pp. 48–51, Dec. 2004.

[27] R. J. Pirkl, K. A. Remley, and C. L. Patané, "Reverberation chamber measurement correlation," *IEEE Trans. Electromagn. Compat.*, vol. 54, no. 3, pp. 533–545, Jun. 2012.

[28] X. Chen, "Experimental investigation of the number of independent samples and the measurement uncertainty in a reverberation chamber," *IEEE Trans. Electromagn. Compat.*, vol. 55, no. 5, pp. 816–824, Oct. 2013.

[29] H. G. Krauthäuser, T. Winzerling, and J. Nitsch, "Statistical interpretation of autocorrelation coefficients for fields in mode-stirred chambers," in *Proc. IEEE Int. Symp. Electromagn. Compat.*, vol. 2. Chicago, FL, USA, Aug. 2005, pp. 550–555.

[30] K. Rosengren, P.-S. Kildal, C. Carlsson, and J. Carlsson, "Characterization of antennas for mobile and wireless terminals in reverberation chambers: Improved accuracy by platform stirring," *Microw. Opt. Technol. Lett.*, vol. 30, no. 6, pp. 391–397, Sep. 2001.

[31] O. Lunden and M. Backstrom, "Stirrer efficiency in FOA reverberation chambers. Evaluation of correlation coefficients and chi-squared tests," in *Proc. IEEE Int. Symp. Electromagn. Compat.*, vol. 1. Aug. 2000, pp. 11–16.

[32] X. Chen, P.-S. Kildal, C. Orlenius, and J. Carlsson, "Channel sounding of loaded reverberation chamber for over-the-air testing of wireless devices: Coherence bandwidth versus average mode bandwidth and delay spread," *IEEE Antennas Wireless Propag. Lett.*, vol. 8, pp. 678–681, 2009.

[33] C. L. Holloway, H. A. Shah, R. J. Pirkl, K. A. Remley, D. A. Hill, and J. Ladbury, "Early time behavior in reverberation chambers and its effect on the relationships between coherence bandwidth, chamber decay time, RMS delay spread, and the chamber buildup time," *IEEE Trans. Electromagn. Compat.*, vol. 54, no. 4, pp. 714–725, Aug. 2012.

[34] C. T. A. Johnk, *Engineering Electromagnetic Fields and Waves*. New York, NYY, USA: Wiley, 1988.

[35] C. L. Holloway and E. F. Kuester, "Edge shape effects and quasi-closed form expressions for the conductor loss of microstrip lines," *Radio Sci. J.*, vol. 29, no. 3, pp. 539–559, May/Jun. 1994.
[36] L. Lewin, *Advanced Theory of Waveguides*. London, U.K.: Iliffe and Sons, 1951.
[37] S. I. Ganchev, S. Bakhtiari, and R. Zoughi, "A novel numerical technique for dielectric measurement of generally lossy dielectrics," *IEEE Trans. Instrum. Meas.*, vol. 41, no. 3, pp. 361–365, Jun. 1992.
[38] Joint Committee for Guides in Metrology, "Evaluation of measurement data—Guide to the expression of uncertainty in measurement," Int. Bureau Weights Measures, Sèvres, France, Tech. Rep. JCGM 100:2008, Sep. 2008.
[39] K. A. Remley, C.-M. J. Wang, D. F. Williams, J. J. aan den Toorn, and C. L. Holloway, "A significance test for reverberation-chamber measurement uncertainty in total radiated power of wireless devices," *IEEE Trans. Electromagn. Compat.*, vol. 58, no. 1, pp. 207–219, Feb. 2016.
[40] J. A. Jargon, D. F. Williams, T. M. Wallis, D. X. LeGolvan, and P. D. Hale, "Establishing traceability of an electronic calibration unit using the NIST microwave uncertainty framework," in *79th ARFTG Conf. Dig.*, Montreal, QC, Canada, Jun. 2012, pp. 32–36.
[41] X. Chen, "Generalized statistics of antenna efficiency measurement in a reverberation chamber," *IEEE Trans. Antennas Propag.*, vol. 62, no. 3, pp. 1504–1507, Mar. 2014.

Damir Senic received the M.Sc. and Ph.D. degrees from the Faculty of Electrical Engineering, Mechanical Engineering and Naval Architecture, University of Split, Split, Croatia, in 2008 and 2014, respectively.

He is currently with the National Institute of Standards and Technology, Communications Technology Laboratory, University of Colorado Boulder, Boulder, CO, USA, as a Post-Doctoral Research Associate through Professional Research Experience Program. His current research interests include millimeter-wave radio communications, over-the-air measurements in reverberation chambers at millimeter wave and microwave frequencies, electromagnetic compatibility, and the bioeffects of EM fields.

Dr. Senic received the Richard E. Merwin Award from the IEEE Computer Society for exemplary involvement in IEEE activities and excellent academic achievement in 2013. From 2013 to 2014, he was a Guest Researcher with the National Institute of Standards and Technology, Boulder, CO, USA, where he was involved in human exposure and wireless communications aspects of electromagnetic wave absorption in dissipative objects inside reverberant environments. In 2016, he was elected as a Distinguished Reviewer of the IEEE TRANSACTIONS ON ELECTROMAGNETIC COMPATIBILITY.

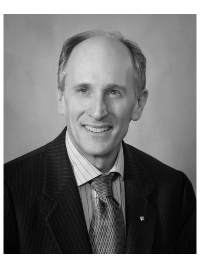

Dylan F. Williams (M'80–SM'90–F'02) received the Ph.D. in electrical engineering from the University of California, Berkeley, CA, USA, in 1986.

He joined the Electromagnetic Fields Division with the National Institute of Standards and Technology, Boulder, CO, USA, in 1989, where he was developed electrical waveform and microwave metrology. He has authored over 100 technical papers.

Dr. Williams was a recipient of the Department of Commerce Bronze and Silver Medals, the Astin Measurement Science Award, two Electrical Engineering Laboratory's Outstanding Paper Awards, three Automatic RF Techniques Group Best Paper Awards, the ARFTG Automated Measurements Technology Award, the IEEE Morris E. Leeds Award, the European Microwave Prize, and the 2013 IEEE Joseph F. Keithley Award. He also served as the Editor of the IEEE TRANSACTIONS ON MICROWAVE THEORY AND TECHNIQUES from 2006 to 2010 and as the Executive Editor of the IEEE TRANSACTIONS ON TERAHERTZ SCIENCE AND TECHNOLOGY. He is currently a President-Elect of the IEEE Microwave Theory and Techniques Society.

Kate A. Remley (S'92–M'99–SM'06–F'13) was born in Ann Arbor, MI. She received the Ph.D. degree in electrical and computer engineering from Oregon State University, Corvallis, OR, USA, in 1999.

From 1983 to 1992, she was a Broadcast Engineer in Eugene, OR, USA. She was a Chief Engineer of AM/FM broadcast station KEED/KSND from 1989 to 1991. In 1999, she joined the RF Technology Division with the National Institute of Standards and Technology, Boulder, CO, USA, as an Electronics Engineer. She is currently the Leader with the Metrology for Wireless Systems Group, NIST, where her current research interests include the development of calibrated measurements for microwave and millimeter-wave wireless systems, characterizing the link between nonlinear circuits and system performance, and developing standardized test methods for RF equipment used by the public-safety community.

Dr. Remley is a member of the Oregon State University Academy of Distinguished Engineers. She was a recipient of the Department of Commerce Bronze and Silver Medals and an ARFTG Best Paper Award. She was the Chair of the MTT-11 Technical Committee on Microwave Measurements from 2008 to 2010 and the Editor-in-Chief of the *IEEE Microwave Magazine* from 2009 to 2011, and is the Chair of the MTT Fellow Committee. She is a Distinguished Lecturer for the IEEE Electromagnetic Compatibility Society from 2016 to 2018.

Chih-Ming Wang received the Ph.D. degree in statistics from Colorado State University, Fort Collins, CO, USA, in 1978.

Since 1988, he has been with the Statistical Engineering Division, National Institute of Standards and Technology, Boulder, CO, USA. He has authored over 90 journal articles. His current research interests include statistical metrology and the application of statistical methods to physical sciences.

Dr. Wang is a fellow of the American Statistical Association (ASA). He was a recipient of the Department of Commerce Silver Medal, Bronze Medal, the NIST Allen V. Astin Measurement Science Award, and several awards from ASA.

Christopher L. Holloway (S'86–M'92–SM'04–F'10) received the B.S. degree from the University of Tennessee at Chattanooga, Chattanooga, TN, USA, in 1986, and the M.S. and Ph.D. degrees in electrical engineering from the University of Colorado at Boulder, Boulder, CO, USA, in 1988 and 1992, respectively.

During 1992, he was a Research Scientist with Electro Magnetic Applications, Inc., Lakewood, CO, USA. His responsibilities included theoretical analysis and finite-difference time-domain modeling of various electromagnetic problems. From 1992 to 1994, he was with the National Center for Atmospheric Research (NCAR), Boulder, where he was involved in wave propagation modeling, signal processing studies, and radar systems design. From 1994 to 2000, he was with the Institute for Telecommunication Sciences, U.S. Department of Commerce, Boulder, where he was involved in wave propagation studies. Since 2000, he has been with the National Institute of Standards and Technology, Boulder, where he was focused on electromagnetic theory. He is currently the Graduate Faculty with the University of Colorado at Boulder. His current research interests include electromagnetic field theory, wave propagation, guided wave structures, remote sensing, numerical methods, metamaterials, measurement techniques, EMC/EMI issues, and atom-based metrology.

Dr. Holloway is a member of URSI Commissions A, B, and E. He was the Chairman for the Technical Committee on Computational Electromagnetics (TC-9) with the IEEE Electromagnetic Compatibility Society from 2000 to 2005, served as the Co-Chair for the Technical Committee on Nano-Technology and Advanced Materials (TC-11) with the IEEE EMC Society from 2006 to 2011, and served as an IEEE Distinguished Lecturer for the EMC Society from 2004 to 2006. He is currently serving as the Chair for US Commission A with the International Union of Radio Science and is an Associate Editor of the IEEE TRANSACTIONS ON ELECTROMAGNETIC COMPATIBILITY.

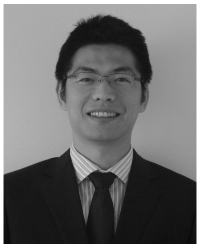

Zhenchao Yang (S'12–M'16) received the Bachelor of Engineering degree in electrical engineering, the Bachelor of Business Administration degree, and the Master of Science degree in electrical engineering from the University of Electronic Science and Technology of China, Chengdu, China, in 2007 and 2010, respectively, and the Ph.D. degree in electrical engineering from Brigham Young University, Provo, UT, USA, in 2015.

He is currently a Sr. RF Design Engineer with Starkey Hearing Technologies, Eden Prairie, MN, USA. He has authored or co-authored over 10 papers in referred journals and conferences. He has 2 U.S. patents and 1 China patent granted and 4 U.S. patent applications. His current research interests include phased arrays, planar and compact antennas, wireless communications, bioelectromagnetics, and microwave circuits.

Dr. Yang is a member of Eta Kappa Nu. He was a recipient of the 2014 Utah NASA EPSCoR Research Student Award and Honorable Mention in the 2014 IEEE International AP-S Symposium Student Paper Competition. He serves as a reviewer for Proceedings of the IEEE, the IEEE TRANSACTIONS ON AEROSPACE AND ELECTRONIC SYSTEMS, the *IEEE Antennas and Wireless Propagation Letters*, the *IEEE Antennas and Propagation Magazine*, *IET Microwave, Antennas and Propagation*, and the *International Journal of Satellite Communications and Networking*. He also served as a Session Co-Chair for the 2014 IEEE International AP-S Symposium.

Karl F. Warnick (SM'04–F'13) received the B.S. (*magna cum laude*) degree in electrical engineering and mathematics with University Honors and the Ph.D. degree in electrical engineering from Brigham Young University (BYU), Provo, UT, USA, in 1994 and 1997, respectively.

From 1998 to 2000, he was a Post-Doctoral Research Associate and a Visiting Assistant Professor with the Center for Computational Electromagnetics, University of Illinois at Urbana-Champaign, Champaign, IL, USA. Since 2000, he has been a Faculty Member with the Department of Electrical and Computer Engineering, BYU, where he is currently a Professor. From 2005 to 2007, he was a Visiting Professor with the Technische Universität München, Munich, Germany. He has authored many scientific articles and conference papers on electromagnetic theory, numerical methods, remote sensing, antenna applications, phased arrays, biomedical devices, and inverse scattering, and has also coauthored the books *Problem Solving in Electromagnetics, Microwave Circuits, and Antenna Design for Communications Engineering* (Artech House, 2006), *Numerical Analysis for Electromagnetic Integral Equations* (Artech House, 2008), and *Numerical Methods for Engineering: An Introduction Using MATLAB and Computational Electromagnetics Examples* (Scitech, 2010).

Dr. Warnick has served as a member of the Antennas and Propagation Society. He has been a Technical Program Committee Member of the International Symposium on Antennas and Propagation for several years. He was a recipient of the National Science Foundation Graduate Research Fellowship, the Outstanding Faculty Member award for Electrical and Computer Engineering, the BYU Young Scholar Award, the Ira A. Fulton College of Engineering and Technology Excellence in Scholarship Award, and the BYU Karl G. Maeser Research and Creative Arts Award. He has served as the Co-Chair of the Education Committee, a Senior Associate Editor of the IEEE TRANSACTIONS ON ANTENNAS AND PROPAGATION, and the Technical Program Co-Chair for the Symposium in 2007.